Nonlinear contact mechanics based on ring-down experiments with quartz crystal resonators

Steffen Berg
Max-Planck-Institute for Polymer Research, Ackermannweg 10, 55128 Mainz, Germany

Thomas Prellberg
Institute of Theoretical Physics, Technical University Clausthal, Arnold-Sommerfeld Str. 6,38678 Clausthal-Zellerfeld

Diethelm Johannsmann[a)]
Institute of Theoretical Physics, Technical University Clausthal, Arnold-Sommerfeld Str. 6,38678 Clausthal-Zellerfeld

(Received 25 June 2002; accepted 24 September 2002)

We report on the explicit derivation of a nonlinear spring constant and a nonlinear friction coefficient describing the interaction between an oscillating quartz plate and a tip touching its surface. The analysis is based on ring-down experiments. After the electrical excitation is turned off, the decay of the oscillation shows an amplitude-dependent resonance frequency and decay rate. This "chirp" does not occur when the quartz plate is out of contact. The chirp and the nonlinear decay rate are converted to a nonlinear spring constant $\kappa_1(x)$ and a nonlinear friction coefficient $\xi_1(\dot{x})$ by means of a perturbation analysis. © *2003 American Institute of Physics.*
[DOI: 10.1063/1.1523647]

I. INTRODUCTION

In contact mechanics, some often encounters large local stresses due to the small size of the asperities supporting the contact. The size of the asperities adjusts itself such that the stress is just below the yield stress. Otherwise, the size of the local contact area grows via plastic deformation. Among the most striking consequences of nonlinear contact mechanics are the laws of sliding friction, where the friction force is largely independent of sliding speed.[1] This greatly contrasts hydrodynamic friction, where the drag force is proportional to speed according to the Stokes law.

Nonlinear force–displacement relations are also often encountered when contact is made between a sharp tip—for instance, the tip of an atomic force microscope (AFM)[2]—and a substrate. In this case, one has a single-asperity contact which, under severe conditions of cleanliness, may be molecularly well defined. Experiments of this kind have evolved to a field of their own termed "nanotribology."[3] Piezodrives providing for nanopositioning are essential components of these instruments. While they are extremely accurate, these devices do not usually reach high sliding speeds. The same holds for the surface forces apparatus, where a single-asperity contact is achieved between two molecularly flat mica sheets.[4]

Recently, quartz-crystal resonators[5] have been suggested as tools for microtribology.[6–8] Quartz resonators allow for high speeds and accurate positioning at the same time due to their high resonance frequency. Of course one deals with an oscillatory rather than a steady motion. In our previous work, we have monitored the shifts in resonance frequency and bandwidth of the quartz resonator while having small spheres approach its surface. The resonances were probed passively by connecting the electrodes of the resonator to an impedance analyzer and performing frequency sweeps. The conductance spectra were fitted with resonance curves. When the two bodies are tightly locked, the shifts in frequency and bandwidth are reasonably well explained in terms of the Hertz model.[6] Frequently, a peak in bandwidth is seen when the sphere just barely touches the quartz surface. This maximum is caused by friction.[6–8] Implicitly assumed in the analysis of these experiments is a linear friction force–speed relation. For a linear friction force–speed relation, the equation of motion corresponds to a damped harmonic oscillator. The fact that the data traces on the impedance analyzer could be fitted well with resonance curves justifies this analysis to some extent. On the other hand, a linear force–speed relation is not expected. Possibly, the technique was not sensitive enough to detect nonlinear components of the friction force.

Here, we report on a refined approach, optimized for the detection of nonlinear force–displacement relations. In order to have more direct access to the motion of the quartz plate, we have performed "ring-down" experiments (Fig. 1) rather than frequency sweeps.[9] The quartz plate is excited at its resonance frequency and the excitation is interrupted periodically. The free decay of the oscillation is visualized with an oscilloscope. Importantly, frequency and decay rate vary during the decay, that is, they depend on the instantaneous amplitude. The amplitude-dependent frequency reflects a nonlinear reaction force.

[a)]Author to whom correspondence should be addressed; present address; Institute of Physical Chemistry, Technical University Clausthal, Arnold-Sommerfeld-Str. 4, 38678 Clausthal-Zellerfeld; electronic mail: johannsmann@pc.tu-clausthal.de

 © 2003 American Institute of Physics

Downloaded 18 Jan 2003 to 140.180.134.111. Redistribution subject to AIP license or copyright, see http://ojps.aip.org/rsio/rsicr.jsp

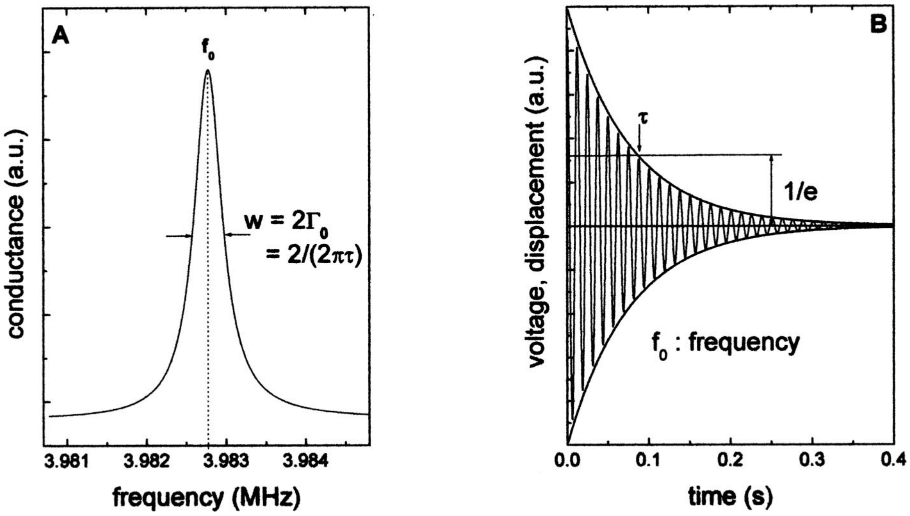

FIG. 1. (A) Resonance curve (B) freely decaying quartz vibration in the time domain. As long as linear force–displacement relations are obeyed, the two representations contain the same information, namely the resonance frequency and the decay rate. In the presence of nonlinearities, the direct visualization of the movement of the quartz plate in the ring down provides a more direct access to the underlying forces.

II. EXPERIMENTAL SETUP

Figure 2 shows a sketch of the experimental setup. We used AT cut quartz-crystal shear resonators (MaxTek Inc., CA) with a fundamental frequency of 4 MHz. The cut is such that the quartz plates are temperature compensated for the third overtone. The quartz plates were flat and optically polished on both sides. On the fundamental at 4 MHz, these quartz usually have poor energy trapping,[10] resulting in a rather broad resonance. At 12 and 20 MHz, the energy trapping is sufficient, yielding resonances with a width of less than 30 Hz. Spheres were approached to the center of the quartz plate using an inertia drive for a coarse approach (PT30, OWIS, Staufen, Germany) and a piezostage for a fine approach (P-732.ZC from Physics Instruments, Waldbronn, Germany). The piezostage has active feedback control with capacitive sensors for distance control. The short-time positioning accuracy is below 1 nm. Two types of approaching surfaces were employed: (a) ceramic spheres (Si_3N_4, Elektroschmelzwerk Kempten, Germany, $r=5$ mm) which had been glued to a rod and (b) glass rods, where one end had been molten to form a droplet, retaining the droplet shape after cooling. The roughness as determined with AFM was below 1 nm root mean square (rms).

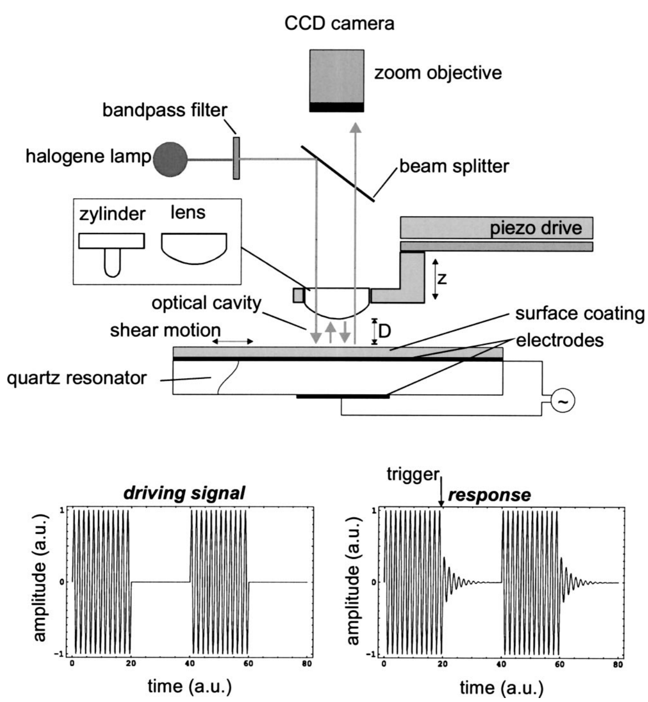

FIG. 2. Sketch of the experimental setup and data acquisition.

The setup contains a normal force transducer with a spring constant of 8600 ± 300 N/m (ELG-H20 from ENTRAN, France) to measure vertical forces. The spring constant is high enough to prevent a jump into contact. The force transducer does not at all affect the MHz motion because of its inertia. The MHz motion causes ultrasound to be radiated into the approaching body. Because the contact range is so small, the probability that reflected sound waves reenter the quartz crystal is negligible. Deep in contact, the normal force always shows a linear increase of the force with piezotravel (Fig. 3), which says that the weakest element is the spring of the force transducer (rather than the Hertzian contact between the sphere and the quartz plate which obeys a force–displacement relation[11] of $F\propto\delta^{3/2}$).

From the finite roughness of the quartz plate (~3 nm rms), one can estimate a typical contact area to be in the range of some square microns. At this point, we do not perform true nanotribology. Nanosized contacts are achieved when the spheres are replaced by AFM or scanning tunneling microscopy tips.[12–14] However, the frequency shifts induced by AFM tips are too small for the analysis described here. In a separate article, we reported on the integration of this setup into a surface force apparatus, where nanoscopic control over the surfaces has indeed been achieved.[8]

The setup was contained in a closed chamber. The experiments were performed at room temperature in a dry nitrogen atmosphere (<6 rH, drying agent: phosphorous pentoxide). The temperature typically varied by approximately 0.2 °C during a measurement, resulting in mechanical drifts of about 0.6 nm/min.

III. SAMPLE PREPARATION

Prior to the experiment, the quartz plates were sonocated in a detergent solution (Hellmanex from Hellma, Müllheim, Germany) and milliQ-water. Gold electrodes were evapo-

Downloaded 18 Jan 2003 to 140.180.134.111. Redistribution subject to AIP license or copyright, see http://ojps.aip.org/rsio/rsicr.jsp

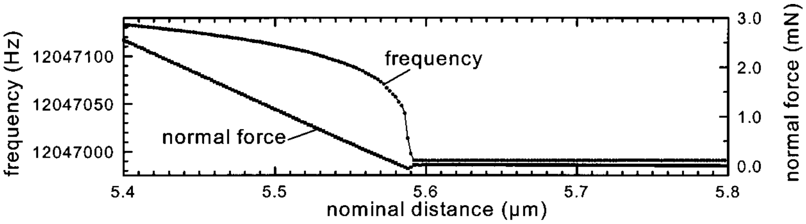

FIG. 3. Frequency shift δf and normal force in a gold–gold contact. At a very small separation, the surfaces show weak attractive forces. During further decrease of the nominal distance, the normal force increases linearly with piezotravel.

rated onto the quartz blanks where adhesion was ensured with a 2 nm thick chromium layer. The top electrode was always connected to the ground in order to avoid potential drops between the gold surface and sphere. The back electrode was keyhole shaped and much thicker ($>$500 nm gold) than the top electrode to achieve energy trapping.[10] The half-band-half-width on the third overtone typically was 30 Hz.

The entire sample chamber was cleaned with ethanol prior to the experiment. In order to check for dust particles in the contact zone, a microscope was integrated into the setup (Fig. 2). We used a halogen lamp with a narrow bandwidth filter (Schott DAD8, $\lambda = 628.2 \pm 5$ nm) coupled into a zoom objective with 40 mm working distance (Opto, Germany) for top illumination. As the opposing surface, we used the transparent glass rod. The space between the upper gold electrode of the quartz resonator and the curved surface of the glass rod acts as an optical cavity leading to Newton's rings in the microscope image.

Figure 4 shows two micrographs with and without contamination by dust particles. In the case of a clean contact, the approach curve [Fig. 4(A)] exhibits a sharp peak in the bandwidth. Figures 4(C) and 4(D) show an experiment where the gold electrodes were covered with silica microspheres (1.5 μm diameter). In this case, the peak in bandwidth is broadened to the extent that it is hardly discernible at all.

IV. DATA ACQUISITION

Prior to the experiment, all quartzes were inspected conventionally with an impedance analyzer (E5100A from Agilent Technologies, Germany). From the conductance spectra, one can determine whether a given mode is regular in appearance [cf. Fig. 1(A)] and well separated from anharmonic side bands.

For the ring-down experiments, the quartz was excited at its resonance frequency by a high-frequency synthesizer (HP3325A, Agilent) which was connected to the electrodes across an electronic switch (mini circuits, 15542 ZAD-3H). The switch (triggered by a Kontron 8201 pulse generator)

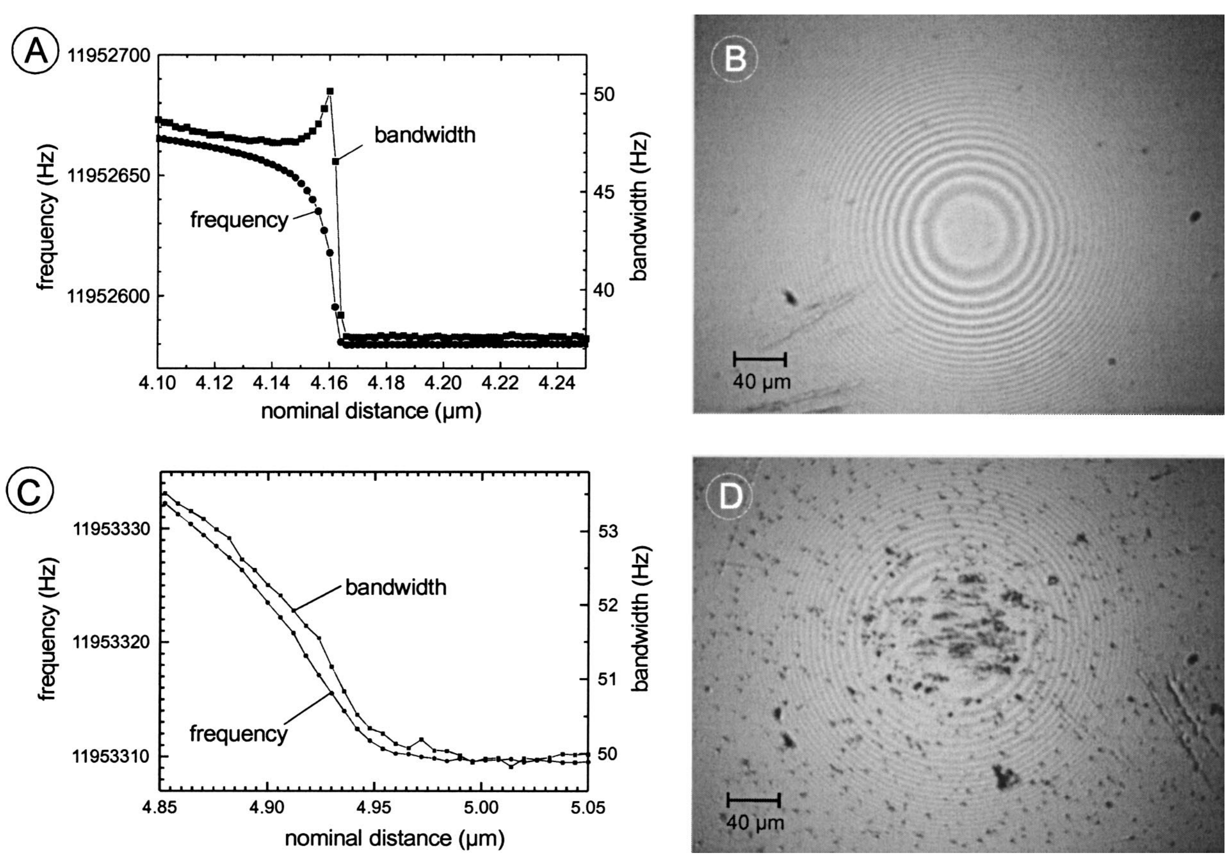

FIG. 4. (A) Approach curve of a round-molded glass rod onto the upper gold electrode of a quartz resonator. Frequency and bandwidth both increase and, at the point of contact, the bandwidth exhibits an additional peak. The microscope image (B) shows that the contact zone is free from contamination with particles. No bandwidth peak is observed (C) when microspheres (1.5 μm diameter) are present in the contact zone (D).

Downloaded 18 Jan 2003 to 140.180.134.111. Redistribution subject to AIP license or copyright, see http://ojps.aip.org/rsio/rsicr.jsp

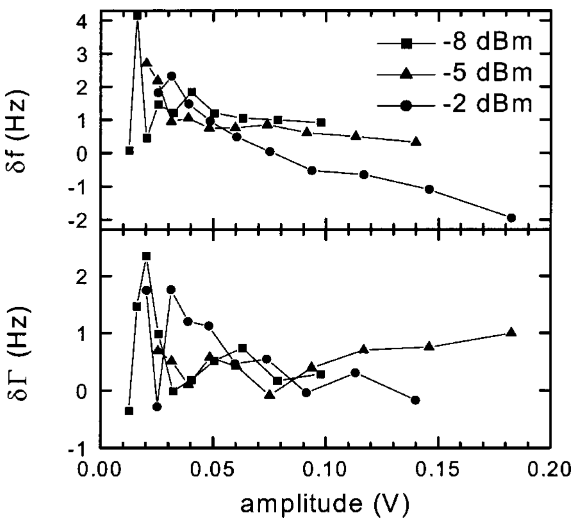

FIG. 5. Amplitude dependence of the frequency shift δf and bandwidth shift $\delta\Gamma$ over the decay of a free oscillating quartz resonator. For drive levels above -5 dB m, the quartz shows intrinsic nonlinearities.

turned the excitation on and off at a rate between of 20 and 100 Hz. The pulse generator also triggered a digital oscilloscope (LeCroy 9351AM) which stored the output voltage of the quartz crystal after the excitation had stopped. The oscillation decayed freely as depicted in Fig. 1(B). Due to the piezoeffect, the current through the electrodes is proportional to the average shear strain in the crystal and, therefore, a direct measure of the movement of the plate. Note, however, that the strain is averaged over the entire active area, which is larger than the typical contact area by a factor of 10^4.

The data were transferred from the digital oscilloscope to a personal computer and numerically analyzed online. Actually, the online analysis limits the speed of data acquisition. Each data set was cut into slices. The total number of slices varied between 10 and 50. A rough initial estimate for the frequency, f, was obtained from a fast Fourier transform. Estimates for the amplitude A and the decay rate $2\pi\Gamma$ were derived from fitting an exponential to the envelope. An estimate for the phase φ was obtained from fitting a cosine to the first few oscillations. In this fit, the phase was the only free parameter; the frequency and the amplitude were kept fixed. With these guess values, a nonlinear Levenberg Marquardt fit[15] was performed. The fit function is $A_i \cos(2\pi f_i t + \varphi_i)\exp(-2\pi\Gamma_i t)$ where the fit parameters are A, f, φ, and Γ. The index i labels the particular slice under consideration. At this point, only the frequencies f_i and the decay rates $2\pi\Gamma_i$ are of further interest. We subtracted the values f_0 and Γ_0 from the freely oscillating quartz and plotted the resulting δf_i and $\delta\Gamma_i$ as function of the amplitude A_i (Fig. 5).

V. INSTRUMENT PERFORMANCE

The typical contact radius is in the order of 10–40 μm. Larger contact areas can be achieved by increasing the size of the sphere. Since we are interested in small contacts, this is not favorable. In addition, a larger contact are increases the bandwidth of the quartz resonator and decreases the amplitude of motion. A smaller contact area, of the sphere of the piezostage on the other hand, introduces less frequency shift. The trade off between these effects results in an optimum radius of curvature of 2–3 mm.

The short-time accuracy of the sphere piezostage is governed by the capacitive elements used for feedback. It is about 1 Å. On longer time scales, there is a thermal drift in the order of 1 nm/min, which limits the repeatability of the approach.

Even in the absence of a mechanical contact the quartz resonator shows intrinsic nonlinearities if the drive power is too high. In Fig. 5, we show δf and $\delta\Gamma$ as a function of the instantaneous amplitude for different driving powers ranging from -8 to -2 dB m. Below a driving power of -5 dB m, there were no intrinsic nonlinearities. A drive power of -5 dB m was, therefore, used in most experiments.

We always display single measurements and did not average over different single scans. At high amplitude, the accuracy of δf and $\delta\Gamma$ is better than 1 Hz. With decreasing amplitude, electronic noise becomes an increasing source of error in the nonlinear fit. At low amplitudes, the accuracy is about 2–5 Hz with occasional outliers.

The maximum data acquisition rate is, in principle, limited by the decay rate of the oscillation, which is of the order of 50 Hz. However, the experiments have to be analyzed online in order to ensure that the driving circuitry always operates at the true resonance frequency. Data analysis takes a few seconds. It was necessary to take 200–500 data points over a vertical range of 1 μm in order to catch all interesting features with sufficient vertical resolution. A typical experiment takes about 1 h.

VI. DERIVATION OF NONLINEAR SPRING CONSTANTS AND FRICTION COEFFICIENTS

As stated in Sec. I, nonlinear terms in the equation of motion are an essential part of solidlike friction. Having found clear evidence of nonlinear behavior when detecting an amplitude-dependent frequency and bandwidth, the question arises as to whether these can be converted into the corresponding nonlinear terms in the equation of motion. This can be done by a perturbation analysis. The formalism is based Ref. 16. We start out from an equation of motion of the form

$$m\ddot{x}+(\xi_0+\xi_1(\dot{x}))\cdot\dot{x}+(\kappa_0+\kappa_1(x))x=0, \tag{1}$$

where m, ξ_0, and κ_0 are the mass, the friction coefficient, and the spring constant of the freely oscillating quartz, respectively. m is one half of the mass of the active portion of the crystal, that is, $m=A_{\mathrm{el}}Z_q/(4f_0)$, with A_{el} as the electrode area, $Z_q=8.8\times10^6$ kg m^{-2} s^{-1} as the acoustic impedance of AT-cut quartz, and f_0 as the fundamental frequency. The parameters $\xi_1(\dot{x})$ and $\kappa_1(x)$ are a nonlinear friction coefficient and a nonlinear spring constant (chosen such that $\xi_1(0)=0$ and $\kappa_1(0)=0$). The dot is the derivative with respect to time, t. Note that Eq. (1) is not the most general form of a weakly nonlinear system because cross terms containing both x and $\dot{x}$ are excluded. Further, we assume that ξ and κ only depend on the state of the system at that same time. ξ and κ are non-hysteretic. (The entire system may be hysteretic if the nonlinearilies are too strong.)

Downloaded 18 Jan 2003 to 140.180.134.111. Redistribution subject to AIP license or copyright, see http://ojps.aip.org/rsio/rsicr.jsp

It is our goal to explicitly derive $\xi_1(\dot{x})$ and $\kappa_1(x)$ from the amplitude-dependent damping $\Gamma(A)$ and frequency shift $\delta f(A)$. We use the "two-timing approximation" for weakly nonlinear oscillators, as described in Ref. 16. This approximation is based on the observation that one can identify two different time scales in the problem. We introduce the new parameters $\gamma_0=\xi_0/m$, $\gamma_1=\xi_1/m$, ${\omega_0}^2=\kappa_0/m$, and ${\omega_1}^2=\kappa_1/m$ and write Eq. (1) as

$$\ddot{x}+{\omega_0}^2x+[(\gamma_0+\gamma_1(\dot{x}))\cdot\dot{x}+{\omega_1}^2(x)x]=0. \tag{2}$$

The term in the square brackets can be interpreted as a perturbation of the harmonic oscillator equation $\ddot{x}+{\omega_0}^2x=0$. The two times scales are described by the dimensionless times $\theta=\omega_0 t$ and $T=\gamma_0 t$. Introducing the small parameter $\varepsilon=\gamma_0/\omega_0$ and substituting θ for t leads to

$$x''+x+\varepsilon h(x,x')=0, \tag{3}$$

with the primes denoting differentiation with respect to θ. From Eq. (2), it follows that $h(x,x')$ is here given by

$$h(x,x')=\alpha(x')x'+\beta(x)x \tag{4a}$$

with

$$\alpha(x')=1+\gamma_1(\omega_0 x')/\gamma_0 \quad \text{and} \quad \beta(x)={\omega_1}^2(x)/(\gamma_0\omega_0). \tag{4b}$$

Regardless of the specifics of $h(x,x')$, the problem at hand is now its determination from the measured amplitude-dependent damping $\Gamma(A)$ and frequency shift $\delta f(A)$. We use the two-timing approximation for weakly nonlinear oscillators,[16] which is based on a first-order perturbation calculation in the small parameter $\varepsilon=\gamma_0/\omega_0$. Starting with the Ansatz

$$x(\theta)=A(T)\cos(\theta+\phi(T)), \tag{5}$$

where $A(T)$ and $\phi(T)$ are a *slowly* varying amplitude and a *slowly* varying phase, respectively, one can show that the following time-averaged equations hold:

$$\frac{dA}{dT}=\frac{1}{2\pi}\int_0^{2\pi}h(A\cos(\theta),-A\sin(\theta))\sin\theta\,d\theta \tag{6a}$$

and

$$A\frac{d\phi}{dT}=\frac{1}{2\pi}\int_0^{2\pi}h(A\cos(\theta),-A\sin(\theta))\cos\theta\,d\theta. \tag{6b}$$

For convenience, the derivation from Ref. 16 is reproduced in Appendix A.

At this point, it is natural to ask under which assumptions one can invert the system (6), or in other words, what can be said about $h(x,x')$ given the measurements of $A(T)$ and $\phi(T)$. In particular, this leads to two important questions about the model assumptions underlying Eq. (1): are these assumptions consistent with the measured data [existence of an inversion of Eq. (6)], and could there be other assumptions leading to the same measured data [uniqueness of the inversion of Eq. (6)].

Due to the appearance of integrals in Eqs. (6a) and (6b) $A(T)$ and $\phi(T)$ are given by weighted averages of $h(x,x')=h(x,\dot{x}/\omega_0)$ over the ellipse $x^2+\dot{x}^2/{\omega_0}^2=A^2$. It follows that inversion is not possible without further assumptions *unless one can vary* ω_0. As this is not possible for the quartz resonators considered here, we proceed with discussing further assumptions, which make an inversion possible. Letting ourselves be guided by the structure of Eq. (1), we write $h(x,x')$ as

$$h(x,x')=\alpha(x,x')x'+\beta(x,x')x, \tag{7}$$

where $\alpha(x,x')$ and β(x,x′) can be related to the nonlinear friction coefficient and the nonlinear spring constant, respectively, and do not yet exclude the possibility of cross terms containing both x and $x'=\dot{x}/\omega_0$.

To achieve simplification, we now assume invariance of $\alpha(x,x')$ and $\beta(x,x')$ under change of sign of x and x'. This assumption is satisfied by Eq. (1) if ξ_1 and κ_1 are even functions of x and $\dot{x}$, respectively. From this, it follows that the system (6) decouples in the sense that Eq. (6a) only contains the term $\alpha(x,x')\cdot x'$ and Eq. (6b) only contains $\beta(x,x')\cdot x$. Because of the invariance under change of sign, one can also restrict the upper limit of integration to $\pi/2$ and one obtains

$$-\frac{1}{A}\frac{dA}{dT}=\frac{2}{\pi}\int_0^{\pi/2}\alpha(A\cos(\theta),-A\sin(\theta))\sin^2\theta\,d\theta \tag{8a}$$

and

$$\frac{d\phi}{dT}=\frac{2}{\pi}\int_0^{\pi/2}\beta(A\cos(\theta),-A\sin(\theta))\cos^2\theta\,d\theta. \tag{8b}$$

The left-hand sides can readily be identified with the damping $\Gamma(A)$ and frequency shift $\delta f(A)$ via

$$2\pi\Gamma(A)=-\frac{1}{A}\frac{dA}{dt}=-\frac{\gamma_0}{A}\frac{dA}{dT}$$

and

$$2\pi\delta f(A)=\frac{d\phi}{dt}=\gamma_0\frac{d\phi}{dT}. \tag{9}$$

In doing so, we casually equate functions of A with functions of T (or t), which however is possible if $A(t)$ is strictly decreasing in time.

The main conclusion so far is that assuming Eq. (7) and invariance under change of sign, the nonlinear friction coefficient affects *only* the damping $\Gamma(A)$ and the nonlinear spring constant affects *only* the frequency shift $\delta f(A)$.

As the right-hand sides of Eqs. (8a) and (8b) correspond to weighted averages of $\alpha(x,x')$ and $\beta(x,x')$ over $x^2+x'^2=A^2$, there are many different $\alpha(x,x')$ and $\beta(x,x')$ which give rise to the same $\Gamma(A)$ and $\delta f(A)$. In order to obtain a unique inversion, one therefore needs to impose further restrictions.

One such restriction is given by assuming a velocity-dependent friction coefficient and position-dependent spring constant as in Eq. (4a) with $\alpha(x')$ and $\beta(x)$ even functions in x' and x. (We emphasize that this choice needs to be made on physical modeling grounds, as it is mathematically rather arbitrary; we could equally well have chosen a position-dependent friction coefficient, for example.) It follows that

Downloaded 18 Jan 2003 to 140.180.134.111. Redistribution subject to AIP license or copyright, see http://ojps.aip.org/rsio/rsicr.jsp

$$\Gamma(A)=\frac{\gamma_0}{\pi^2}\int_0^{\pi/2}\alpha(A\sin\theta)\sin^2\theta\,d\theta$$

$$=\frac{\gamma_0}{4\pi}+\frac{1}{\pi^2}\int_0^{\pi/2}\gamma_1(\omega_0 A\sin\theta)\sin^2\theta\,d\theta \tag{10a}$$

and

$$\delta f(A)=\frac{\gamma_0}{\pi^2}\int_0^{\pi/2}\beta(A\sin\theta)\sin^2\theta\,d\theta$$

$$=\frac{1}{\pi^2\omega_0}\int_0^{\pi/2}\omega_1{}^2(A\sin\theta)\sin^2\theta\,d\theta, \tag{10b}$$

where in Eq. (10b), we have changed the integration variable from θ to $\theta/2-\theta$. The integral transforms in Eq. (10a) and (10b) have identical structure and can be explicitly inverted, as shown in Appendix B. We obtain

$$\gamma_0+\gamma_1(\dot{x})=2\pi\int_0^{\pi/2}\left[3\Gamma\left(\frac{\dot{x}}{\omega_0}\sin\theta\right)+\frac{\dot{x}}{\omega_0}\sin\theta\;\Gamma'\left(\frac{\dot{x}}{\omega_0}\sin\theta\right)\right]\sin^3\theta\,d\theta, \tag{11a}$$

and

$$\omega_1{}^2(x)=2\pi\omega_0\int_0^{\pi/2}[3\,\delta f(x\sin\theta)+x\sin\theta\;\delta f'(x\sin\theta)]\sin^3\theta\,d\theta, \tag{11b}$$

where the primes denote differentiation.

Equations (10) and (11) now provide two different ways of numerical determination of $\gamma_1(\dot{x})$ and $\omega_1{}^2(x)$ from the set of data points $\{(A_i,\Gamma_i=\Gamma(A_i),\delta f_i=\delta f(A_i))|i=1,\ldots,N\}$. We can either discretize Eqs. (10a) and (10b) and invert the resulting matrix numerically, or directly discretize Eqs. (11a) and (11b).

To discretize Eqs. (10a) and (10b), we approximate $\gamma_1(\dot{x})$ and $\omega_1{}^2(x)$ by piecewise constant functions, i.e., we set $\gamma_1(\dot{x})=\gamma_{1,i}$ for $\dot{x}\in(\dot{x}_{i-1},\dot{x}_i)=(\omega_0 A_{i-1},\omega_0 A_i)$ and $\omega_1{}^2(x)=\omega_{1,i}{}^2$ for $x\in(A_{i-1},A_i)$ (with $A_0=0$). It follows that for $i=1,\ldots,N$:

$$\Gamma_i\approx\frac{\gamma_0}{4\pi}+\frac{1}{\pi^2}\sum_{j=1}^{i}\gamma_{1,j}\int_{\arcsin(A_{j-1}/A_i)}^{\arcsin(A_j/A_i)}\sin^2\theta\,d\theta$$

$$=\frac{\gamma_0}{4\pi}+\frac{1}{\pi^2}\sum_{j=1}^{i}\gamma_{1,j}\left[-\frac{\theta}{2}\sqrt{1-\theta^2}+\frac{1}{2}\arcsin\theta\right]_{A_{j-1}/A_i}^{A_j/A_i} \tag{12a}$$

and

$$\delta f_i\approx\frac{1}{\pi^2\omega_0}\sum_{j=1}^{i}\omega_{1,j}{}^2\int_{\arcsin(A_{j-1}/A_i)}^{\arcsin(A_j/A_i)}\sin^2\theta\,d\theta$$

$$=\frac{1}{\pi^2\omega_0}\sum_{j=1}^{i}\gamma_{1,j}{}^2\left[-\frac{\theta}{2}\sqrt{1-\theta^2}+\frac{1}{2}\arcsin\theta\right]_{A_{j-1}/A_i}^{A_j/A_i}. \tag{12b}$$

As these matrix equations are triangular, this leads to a straightforward calculation of $\gamma_{1,j}$ and $\omega_{1,i}{}^2$.

To discretize Eqs. (11a) and (11b), we approximate $\Gamma(A)$ and $\delta f(A)$ by piecewise linear functions. Setting $\Gamma(A)=\Gamma_{i-1}+(\Gamma_i-\Gamma_{i-1})/(A_i-A_{i-1})(A-A_{i-1})$ for $A\in(A_{i-1},A_i)$ (with $A_0=0$), we obtain

$$\gamma_0+\gamma_{1,i}\approx 2\pi\sum_{j=1}^{i}\int_{\arcsin(A_{j-1}/A_i)}^{\arcsin(A_j/A_i)}\left[3\frac{\Gamma_{j-1}A_j-\Gamma_jA_{j-1}}{A_j-A_{j-1}}+4A_i\sin\theta\frac{\Gamma_j-\Gamma_{j-1}}{A_j-A_{j-1}}\right]\sin^3\theta\,d\theta,$$

$$=2\pi\sum_{j=1}^{i}\left[-\frac{\Gamma_{j-1}A_j-\Gamma_jA_{j-1}}{A_j-A_{j-1}}(2+\theta^2)\sqrt{1-\theta^2}+A_i\frac{\Gamma_j-\Gamma_{j-1}}{A_j-A_{j-1}}\left(\frac{3}{2}\arcsin\theta-\theta\frac{3+2\theta^2}{2}\sqrt{1-\theta^2}\right)\right]_{A_{j-1}/A_i}^{A_j/A_i}. \tag{13a}$$

Proceeding *mutatis mutandum* with $\delta f(A)$, we obtain

$$\omega_{1,i}{}^2\approx 2\pi\omega_0\sum_{j=1}^{i}\left[-\frac{\delta f_{j-1}A_j-\delta f_jA_{j-1}}{A_j-A_{j-1}}(2+\theta^2)\sqrt{1-\theta^2}+A_i\frac{\delta f_j-\delta f_{j-1}}{A_j-A_{j-1}}\left(\frac{3}{2}\arcsin\theta-\theta\frac{3+2\theta^2}{2}\sqrt{1-\theta^2}\right)\right]_{A_{j-1}/A_i}^{A_j/A_i}. \tag{13b}$$

We caution here that the assumption of piecewise constant or linear functional behavior is a simplification. One can naturally refine the numerical calculation by using smooth splines, a fitted curve through the data points, or an interpolation polynomial, depending on the quantity and quality of the measured data.

Applying Eqs. (11) and (13) to the same dataset, one obtains very similar results. The differences are less than 2%. In Figs. 6 and 7, we used Eqs. (12a) and (12b).

VII. RESULTS

Depending on the type of surfaces, the resonance parameters as function of piezotravel show different features. Upon contact, the resonance frequency and bandwidth increase. For gold–gold contacts, there is a peak in the bandwidth right at contact. In Fig. 6, we plot δf_i and $\delta\Gamma_i$ as a function of the instantaneous amplitude A_i at three characteristic points of the approach curve which are ‘‘out of contact’’, ‘‘on top of the bandwidth peak’’, and ‘‘deep in contact’’. By deep in contact we mean a nominal vertical position about 100–200 nm lower than the initial contact. The first few nanometers of decrease in nominal distance mostly induce plastic deformation of asperities in the contact zone.[8] A further decrease of the nominal distance leads to an increase of the normal load and deforms the weakest vertical spring which is either the quartz plate or the spring of the force transducer. Due to the increase of the normal load, the sphere elastically

Downloaded 18 Jan 2003 to 140.180.134.111. Redistribution subject to AIP license or copyright, see http://ojps.aip.org/rsio/rsicr.jsp

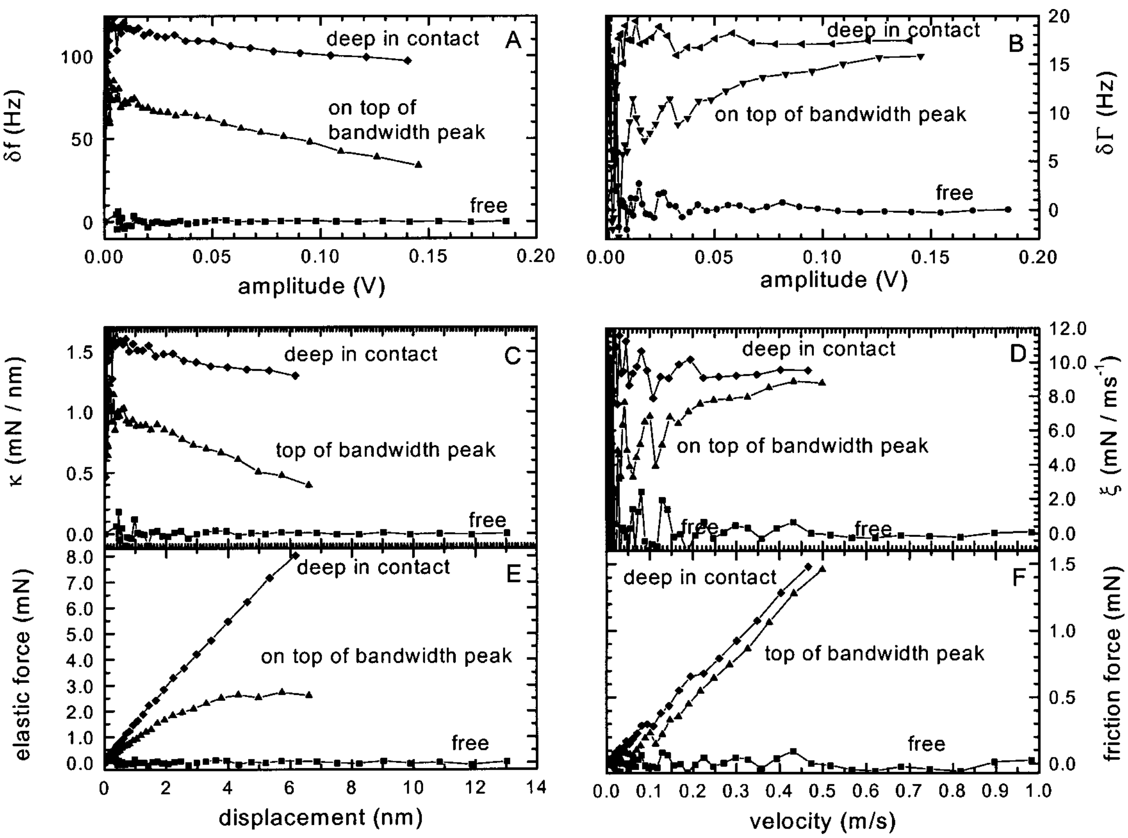

FIG. 6. Frequency shift δf and bandwidth shift $\delta\Gamma$ over 40 sections of a decaying quartz oscillation in a gold–gold contact. Three data sets at different vertical positions are plotted as function of the electrical amplitude (top). Performing the perturbation analysis one obtains the nonlinear spring constant κ_1 and the elastic force as function of the lateral displacement and the nonlinear friction coefficient ξ_1 and the friction force as a function of lateral speed.

deforms which can be well described with the Johnson–Kendall–Roberts (JKR) contact mechanics model.[17]

Deep in contact δf_i and $\delta\Gamma_i$ approach an amplitude-independent behavior. Figures 6(C) and 6(D) show the results of the perturbation analysis, which are the nonlinear spring constant κ_1 and the nonlinear friction coefficient ξ_1 as a function of displacement and speed, respectively. Note that there are two sources for an increase in δf and $\delta\Gamma$: Friction processed in the contact zone and the emission of sound waves.[6,8,20] The latter has no amplitude dependence and, therefore, produces a constant offset. The data do not allow a straightforward separation of effects originating from friction processes in the contact zone and from sound waves. In principle, such a separation might be feasible based on the variation of both effects with vertical pressure.[17] In particular, at the position of the bandwidth peak [Fig. 4(A)] one can assume that most of the dissipation is caused by friction. Only deep in contact κ and ξ are significantly influenced by the emission of sound waves. However, this separation requires additional assumptions. At this point, we do *not* separate the two effects: κ and ξ contain the entire plate–sphere interaction. In Figs. 6(E) and 6(F), we have finally converted the data to a force–displacement relation and a force–speed relation. The maximum displacements and speeds are 20 nm and 1.5 m/s, respectively.

Out of contact both resonance frequency and bandwidth are constant. At the position of the bandwidth peak, the resonance frequency shows a decrease with increasing amplitude resulting in a *sublinear* dependence of the elastic force on displacement. The sublinear force–displacement relation suggests the occurrence of *microslip* in the contact zone which plays an important role in rolling friction.[18] For gold–gold contacts, the bandwidth mostly appears to be independent of the instantaneous amplitude over the entire piezotravel, that is, the friction force depends linearly on the lateral speed. The bandwidth increases with increasing contact area. The linear dependence of the friction force on speed is not in agreement with the speed-independent laws of solidlike friction. Presumably, the high speed of motion results in friction mechanisms, where local minima of the interaction energy are of no consequence. Such mechanisms are sometimes termed "phonon drag".[19] Only at small lateral speeds do we find a deviation from linearity, which we discuss in detail in a separate publication.[20–22]

A contact between a silicon nitride sphere and the bare quartz crystal shows a much different behavior. There is almost no amplitude dependence of either δf_i or $\delta\Gamma_i$, resulting in a linear force–displacement relation and a linear force–speed relation (Fig. 7). Both elastic force and friction force are smaller than for the gold–gold contact. No microslip is observed for the contact between the bare quartz surface and a ceramic sphere. Contacts between hard surfaces exhibit linear elastic behavior and less friction.

Downloaded 18 Jan 2003 to 140.180.134.111. Redistribution subject to AIP license or copyright, see http://ojps.aip.org/rsio/rsicr.jsp

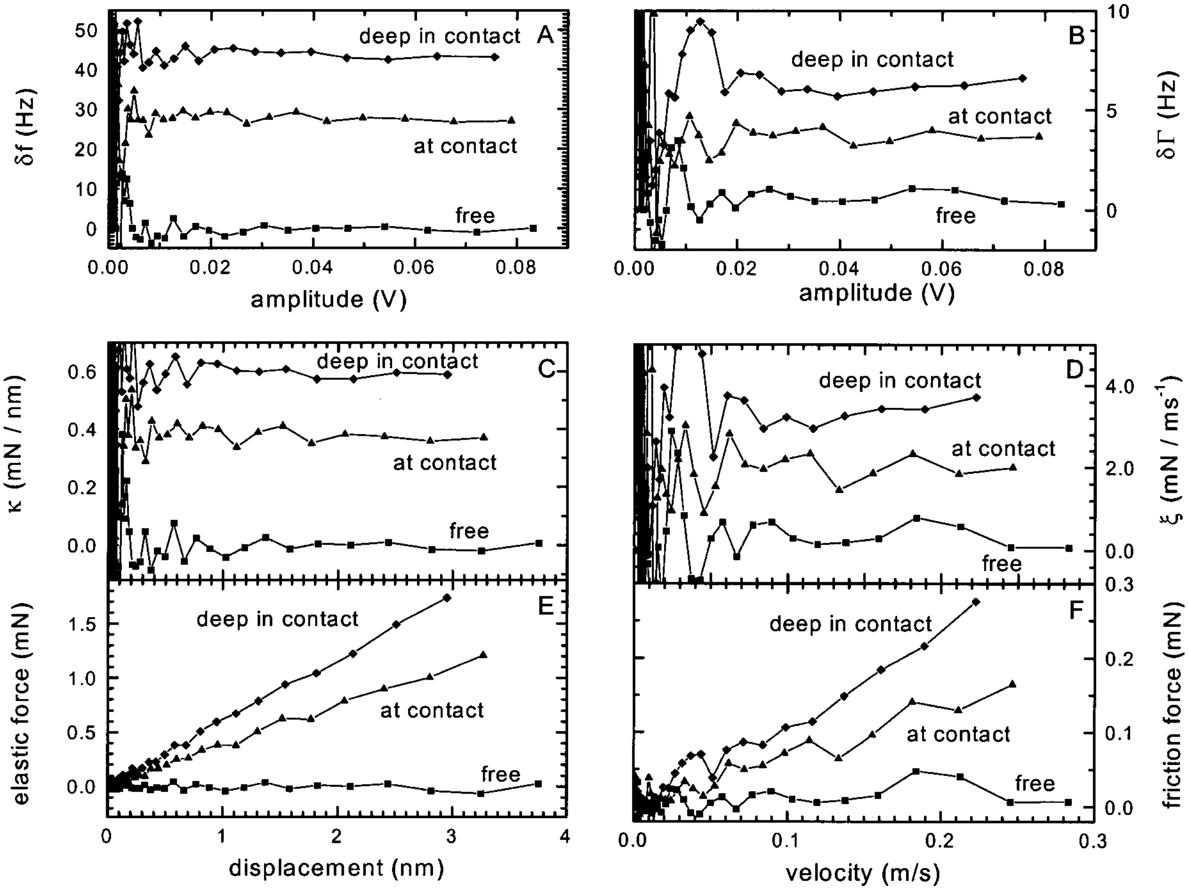

FIG. 7. Same as Fig. 6 for a contact between a bare quartz surface and a Si_3N_4 tip. The elastic force, in this case, is linear in displacement.

ACKNOWLEDGMENTS

The authors thank Alex Laschitsch, Marina Ruths, Hans-Walter Müller, and Martin Müser for helpful discussions.

APPENDIX A: DERIVATION OF THE TIME-AVERAGED EQUATIONS

Given the perturbed harmonic oscillator equation

$$x''+x+\varepsilon h(x,x')=0, \tag{A1}$$

with the primes denoting differentiation with respect to the variable θ, we derive here that for small ε in the two-timing approximation with $T=\varepsilon\theta$, the approximate solution is given by

$$x(\theta)=A(T)\cos(\theta+\phi(T)), \tag{A2}$$

where

$$\frac{dA}{dT}=\frac{1}{2\pi}\int_0^{2\pi} h(A\cos(\theta),-A\sin(\theta))\sin\theta\, d\theta, \tag{A3a}$$

and

$$A\frac{d\phi}{dT}=\frac{1}{2\pi}\int_0^{2\pi} h(A\cos(\theta),-A\sin(\theta))\cos\theta\, d\theta. \tag{A3b}$$

To show this, we insert the Ansatz of Eq. (A2) into Eq. (A1). Terms of order $O(\varepsilon^0)$ vanish. Demanding that terms of order $O(\varepsilon^1)$ vanish, as well, leads to

$$\begin{aligned}&2[A'(T)\sin(\theta+\phi(T))+A(T)\phi'(T)\cos(\theta+\phi(T))]\\&=h(A(T)\cos(\theta+\phi(T))),-A(T)\sin(\theta+\phi(T)).\end{aligned} \tag{A4}$$

The requirement that terms linear in ε vanish is characteristic of the two-timing approximation. Written thus, the function $h(x,x')$ is now a periodic function of $\tau=\theta+\phi(T)$, which we can write as Fourier series

$$h(\tau)=\sum_{k=0}^{\infty} a_k\cos k\tau+\sum_{k=1}^{\infty} b_k\sin k\tau, \tag{A5}$$

where the Fourier coefficients are given by

$$\begin{aligned}a_0&=\frac{1}{2\pi}\int_0^{2\pi} h(\tau)d\tau,\\ a_k&=\frac{1}{\pi}\int_0^{2\pi} h(\tau)\cos k\tau\, d\tau, \quad k\geq 1,\\ b_k&=\frac{1}{\pi}\int_0^{2\pi} h(\tau)\sin k\tau\, d\tau, \quad k\geq 1.\end{aligned} \tag{A6}$$

Hence, Eq. (A4) becomes

$$\begin{aligned}&2[A'(T)\sin\tau+A(T)\phi'(T)\cos\tau]\\&=\sum_{k=0}^{\infty} a_k\cos k\tau+\sum_{k=1}^{\infty} b_k\sin k\tau.\end{aligned} \tag{A7}$$

Downloaded 18 Jan 2003 to 140.180.134.111. Redistribution subject to AIP license or copyright, see http://ojps.aip.org/rsio/rsicr.jsp

Requiring the absence of resonant terms results in $2A'(T) = b_1$ and $2A(T)\phi'(T) = a_1$, which directly leads to Eq. (A3).

APPENDIX B: INVERSION OF THE INTEGRAL EQUATION

We show here that the inverse of

$$a(u) = F(\alpha)(u) = \frac{2}{\pi}\int_0^{\pi/2} \alpha(u \sin\theta)\sin^2\theta \, d\theta \tag{B1}$$

is given as

$$\alpha(v) = G(a)(v) = \int_0^{\pi/2} [3a(v \sin\theta) + v \sin\theta a'(v \sin\theta)]\sin^2\theta \, d\theta \tag{B2}$$

For this, we note first that F maps powers in v to powers in u, as

$$F(v^n)(u) = u^n \frac{2}{\pi}\int_0^{\pi/2} \sin^{n+2}\theta \, d\theta = C_n u^n. \tag{B3}$$

It follows that the inverse transform must satisfy

$$G(u^n)(v) = v^n / C_n. \tag{B4}$$

Using the integral representation of the Beta function[21,22]

$$B(x,y) = 2\int_0^{\pi/2} \sin^{2x-1}\theta \cos^{2y-1}\theta \, d\theta \quad \text{for } x>0 \text{ and } y>0, \tag{B5}$$

we can identify $C_n = B(\mu+3/2,1/2)/\pi$ and obtain $1/C_n$ using $B(x,y) = \Gamma(x)\Gamma(y)/\Gamma(x+y)$ as

$$1/C_n = \frac{n+3}{2} B\left(\frac{n+4}{2}, \frac{1}{2}\right) = (n+3)\int_0^{\pi/2} \sin^{n+3}\theta \, d\theta. \tag{B6}$$

From this, one obtains Eq. (B2) from generating function techniques,[22] using $\Sigma_{n\geqslant 0}(n+3)a_n x^n = [x(d/dx) + 3]\Sigma_{n\geqslant 0} a_n x^n$. The formal proof follows now by verifying that $\alpha(v) = G \circ F(\alpha)(v)$ holds generally.

[1] B. N. J. Perssons, *Sliding Friction* (Springer, Heidelberg, 1998).
[2] E. Meyer, R. M. Overney, and J. Frommer, in *Handbook on Micro/Nano Tribology*, edited by B. Bushan (CRC Press, Boca Raton, 1995), p. 223.
[3] B. Bushan, J. N. Israelachvili, and U. Landman, Nature (London) **374**, 607 (1995).
[4] N. Israelachvili, in *Handbook on Micro/Nano Tribology*, edited by B. Bushan (CRC Press, Boca Raton, 1995), p. 267.
[5] J. Krim, Sci. Am. **1996**, 48 (1996).
[6] A. Laschitsch and D. Johannsmann, J. Appl. Phys. **85**, 3759 (1999).
[7] A. Laschitsch, L. E. Bailey, G. W. Tyndall, C. W. Frank, and D. Johannsmann, Appl. Phys. Lett. **78**, 2601 (2001).
[8] S. Berg, M. Ruths, and D. Johannsmann, Phys. Rev. E **65**, 026119 (2001).
[9] M. Rodahl, F. Hook, A. Krozer, P. Brzezinski, and B. Kasemo, Rev. Sci. Instrum. **66**, 3924 (1995).
[10] V. E. Bottom, *Introduction to Quartz Crystal Unit Design* (Van Nostrand Reinhold, New York, 1982).
[11] J. N. Israelachvili, *Intermolecular and Surface Forces*, 2nd ed. (Academic, London, 1991), p. 328.
[12] J. M. Kim, S. M. Chang, and H. Muramatsu, Appl. Phys. Lett. **74**, 466 (1999).
[13] B. Borovsky, B. L. Mason, and J. Krim, J. Appl. Phys. **88**, 4017 (2000).
[14] A. Sasaki, A. Katsumata, F. Iwata, and H. Aoyama, Jpn. J. Appl. Phys., Part 2 **33**, L547 (1994).
[15] W. H. Press, S. A. Teukolsky, W. T. Vetterling, and B. P. Flannery, *Numerical Recipes in C*, 2nd ed. (Cambridge University Press, Cambridge, UK, 1995).
[16] S. H. Strogatz, *Nonlinear Dynamics and Chaos* (Addison–Wesley, Reading, MA, 1994), p. 215.
[17] S. Berg, D. Johannsmann, and M. Ruths, J. Appl. Phys. (to be published).
[18] K. Johnson, *Contact Mechanics* (Cambridge University Press, New York, 1985).
[19] M. H. Müser, *Atomistic Simulations of Solid Friction*, Lecture Notes in Physics (Springer, Berlin, to be published).
[20] S. Berg and D. Johannsmann (unpublished).
[21] G. B. Arfken and H. J. Weber, *Mathematical Methods for Physicists* (Harcourt/Academic, New York, 2001).
[22] H. S. Wilf, *Generatingfunctionology* (Academic, New York, 1994).

Downloaded 18 Jan 2003 to 140.180.134.111. Redistribution subject to AIP license or copyright, see http://ojps.aip.org/rsio/rsicr.jsp